11th World Congress on Computational Mechanics (WCCM XI)
5th European Conference on Computational Mechanics (ECCM V)
6th European Conference on Computational Fluid Dynamics (ECFD VI)
E. Oñate, J. Oliver and A. Huerta (Eds)

2D AND 3D NUMERICAL SIMULATIONS OF DAMAGE DURING THE FORMATION OF SUCCESSIVE CHIPS WHEN MACHINING THE AERONAUTICAL CFRP COMPOSITES

SOFIANE ZENIA*, LANOUAR BEN-AYED*, MOHAMMED NOUARI* AND ARNAUD DELAMÉZIÈRE*

* Laboratoire d´Energétique et de Mécanique Théorique et Appliquée, LEMTA CNRS-UMR 7563, Université de Lorraine, Ecoles des Mines d'Albi,
GIP-InSIC, 27 rue d'Hellieule, 88100, Saint-Dié-des-Vosges, France.

E-mail: sofiane.zenia@univ-lorraine.fr, lanouar.ben-ayed@univ-lorraine.fr, mohammed.nouari@univ-lorraine.fr, arnaud.delameziere@univ-lorraine.fr

Key Words: *Machining process; FRP composites; Finite-Element analysis; induced-cutting damage; stiffness degradation,.*

Abstract. *A finite element method has been developed to simulate the cutting process of composites containing long carbon fibers and polymer matrix (CFRP composites). A complete mechanical approach has been performed coupling the damage-elastoplastic behavior and stiffness degradation of the composite properties. Moreover, the plasticity caused by permanent deformation, fiber-matrix debonding and matrix cracking has been taken into account. In this work, a unidirectional ply was studied using a meso-scale modelling of damages in composites. The proposed approach is primarily focused on the understanding of interactions between the fiber orientation, machining process and the physical phenomena governing the chip formation process.*

The analysis of the chip formation, cutting forces and the induced damage has been done through 2D and 3D simulations. A VUMAT subroutine, providing the capability for implementing elastoplastic damage models has been used in Abaqus/Explicit. A damage variable has been calculated for each type of damage that appears in the workpiece: fiber breaking, matrix cracking and fiber-matrix debonding.

Satisfactory numerical results have been obtained on an orthogonal cutting application and a good correlation has been found with experimental results, [2,10].

1 INTRODUCTION

Nowadays, the use of FRP composites becomes more attractive in various industrial sectors such as aerospace, naval, and automotive. These materials are characterized by the high mechanical properties (strength, stiffness, …) and light weight. For the environment, the weight gain also goes in the good direction with reducing pollutant emission and energy consummation. However, the heterogeneity and the abrasive nature of fibres make the machinability of these materials more difficult compared to the conventional metals and their alloys. That is why the development of knowledge on the behavior of composites is considered

as a challenging task to manufacturing engineers. Indeed, excessive tool wear and damage induced in the workpiece, as the pullout of fibers, matrix cracking and matrix-fiber debonding, often occur when machining this kind of materials.

Koplev et al. [1], were the first authors to study the mechanisms of chip formation. They have conducted experimental studies on the orthogonal cutting of carbon fiber-reinforced polymer composites (CFRP). The main conclusion of their work is that the fiber orientation plays a key role in the chip formation process. Machining tests on edge trimming and orthogonal cutting of graphite/epoxy composites were conducted by Wang et al. [2] and Arola et al. [3]. These authors found that all aspects of composite material removal were primarily dependent on the fiber orientation. It has been concluded from their work that the chip formation, the cutting forces, and the surface morphology were highly dependent on the fiber orientation. However, the optimization of these parameters only by experimental approaches often requires long and very expensive trials. So, numerical simulation and modelling can be very helpful to characterise and to validate optimal domains of the cutting parameters.

Modelling of machining composites was first developed by Arola and Ramulu [4]. The authors presented a finite element model with a predefined fracture plane to simulate the chip formation in the orthogonal cutting operation. They explained the mechanism of the chip formation which is composed into primary and secondary rupture. Other works have been interested to the mechanisms of chip formation, cutting forces calculation, subsurface induced damage and surface roughness [5-10].

Indeed, the numerical simulation will be then an interesting tool for the analysis of the physics that governs the cutting composites and to study the most influential parameters. It will also help to understand the physical mechanisms governing the formation of the chip and to have a clear idea about the state of the subsurface induced damage in the machined part.

Different models have been used during various investigative works on FRP composites. Micro-mechanical modellings of Gopala Rao et al. [9] proposed a quasi-static approach based on the ABAQUS Explicit software. Lasri et al.[8] and Soldani et al.[9] opted for a macroscopic model where the workpiece is modelled as a homogeneous equivalent material (HEM). Iliescu et al. [10] proposed another work based on Discrete Element Method (DEM) to simulate the mechanisms of chip formation and calculate machining forces in orthogonal cutting of UD-CFRP composites.

In the current investigation, we develop a complete model with different physical aspects of machining composites. The proposed approach is based on a mesomechanic model in which we combine the stiffness degradation effect in the response material behavior, plasticity using the effective stress concept and evolution laws to predict damage initiation and progression during the chip formation process. The model propose a dynamic approach based on ABAQUS EXPLICIT software and a damaged-mechanical behavior was implemented in a 2D and 3D numerical models using a VUMAT subroutine. In this work, the workpiece is modelled as a homogeneous equivalent material (HEM). The model allows a better understanding of the physical phenomena observed during the cutting operation, and give an accurate numerical tool to simulate the real chip formation, cutting forces, and induced subsurface damage by. The obtained numerical results were compared to experiments performed by Iliescu et al. [10].

2 ELASTOPLASTIC DAMAGE MODEL

2.1 Plastic model

The elastic-plastic-damage model is based on the effective stresses concept as shown by Lemaitre and Chaboche [17]. In the current work, the yield function is written considering an isotropic hardening and it is assumed that there is no plastic flow in the fiber direction. The layer is assumed to be in a plane stress situation in the 2D Model, i.e., only σ_{11}, σ_{22}, and σ_{12} are nonzero stresses. While, the layer is assumed to be in three dimensional in the 3D Model. The elasticity domain is defined according to the following plastic activation function:

$$F(\tilde{\boldsymbol{\sigma}},\sigma_y) = f^p(\tilde{\boldsymbol{\sigma}}) - \sigma_y(p) \tag{1}$$

Where f^p is the plastic potential, and σ_y is the current yield stress which represents the isotropic hardening law and is defined in function of the cumulated plastic strain p:

$$\sigma_y(p) = R_0 + R(p) = R_0 + \beta p^{\alpha} \tag{2}$$

Where R_0 is the initial yield stress, and the quantities β and α are the hardening parameters.

The plastic potential function is defined considering a plane stress condition and it does not depend on stresses σ_{11} in the fiber direction because the fiber behaviour is assumed to be elastic brittle under tension or compression:

$$f^p(\tilde{\sigma}) = \sqrt{\tilde{\sigma}_{12}^2 + c^2\tilde{\sigma}_{22}^2} \tag{3}$$

$$f^p(\tilde{\sigma}) = \sqrt{\tilde{\sigma}_{12}^2 + \tilde{\sigma}_{23}^2 + \tilde{\sigma}_{13}^2 + c^2[\tilde{\sigma}_{22}^2 + \tilde{\sigma}_{33}^2]} \tag{4}$$

Where c is a coupling parameter, and the effective stresses are defined as follows:

$$\tilde{\sigma}_{12} = \frac{\sigma_{12}}{1-D_{12}};\ \tilde{\sigma}_{23} = \frac{\sigma_{23}}{1-D_{12}};\ \tilde{\sigma}_{13} = \frac{\sigma_{13}}{1-D_{12}};$$
$$\tilde{\sigma}_{22} = \frac{\langle\sigma_{22}\rangle_+}{1-D_{22}} + \langle\sigma_{22}\rangle_-;\ \tilde{\sigma}_{33} = \frac{\langle\sigma_{33}\rangle_+}{1-D_{22}} + \langle\sigma_{33}\rangle_- \tag{5}$$

Where D_{22}, D_{12} denote damage developed in the transverse direction, and under shear stress condition, respectively. The symbols $\langle\bullet\rangle_-$ and $\langle\bullet\rangle_+$ in equation (5) mean the negative and positive part of $\bullet$, respectively, introduced to model the unilateral effect for the effective transverse stress. The transverse behavior in compression is indefinitely elastoplastic, due to the introduced unilateral effect. So, transverse damage affects the tensile behaviour only.

The effective inelastic part of the deformation is defined by the flow rule (or normality rule) as:

$$\left\{d\tilde{\boldsymbol{\varepsilon}}^p\right\} = d\lambda\frac{\partial F}{\partial\left\{\tilde{\boldsymbol{\sigma}}\right\}} \text{ and } dp = -d\lambda\frac{\partial F}{\partial\sigma_y} = d\lambda \tag{6}$$

Where $d\lambda$ is a nonnegative plastic consistency parameter (plastic multiplier).

The plastic strain increment is obtained from the equivalence principle of the plastic work

increment dW^p presented as follows:

$$dW^p = \tilde{\boldsymbol{\sigma}} : \mathbf{d}\tilde{\boldsymbol{\varepsilon}}^p = \boldsymbol{\sigma} : \mathbf{d}\boldsymbol{\varepsilon}^p \tag{7}$$

In addition, the consistency condition ($dF = 0$), should be satisfied and leads to compute the cumulated plastic increment:

$$dp = \frac{\left\langle \frac{\partial F}{\partial \tilde{\boldsymbol{\sigma}}} \right\rangle \ [\mathbf{C}]}{\left\langle \frac{\partial F}{\partial \tilde{\boldsymbol{\sigma}}} \right\rangle \ [\mathbf{C}] \ \left\{ \frac{\partial F}{\partial \tilde{\boldsymbol{\sigma}}} \right\} \ + \ \frac{\partial \sigma_y}{\partial p}} \{\mathbf{d}\boldsymbol{\varepsilon}\} = \langle \mathbf{a} \rangle \ \{\mathbf{d}\boldsymbol{\varepsilon}\} \tag{8}$$

An algorithm based on a radial returns predictor [18] is implemented in order to return the stresses to the yield surface. In fact, for an increment strain, an initial elastic prediction step is carried out. If the yield function is greater than zero, an iterative correction procedure uses the normal of the last yield surface until the yield function vanishes.

2.2 Damage evolution

In the proposed model, different degradation modes were considered: fiber breakage in traction as well as in compression, matrix cracking and fiber-matrix deboning. In the 2D model, the strain energy density [11-15] of the damaged ply is defined as follow:

$$e_D = \frac{1}{2}\left[\frac{\sigma_{11}^2}{E_{11}^0(1-D_{11})} - \frac{2\nu_{12}^0}{E_{11}^0}\sigma_{11}\sigma_{22} + \frac{\langle \sigma_{22} \rangle_+^2}{E_{22}^0(1-D_{22})} + \frac{\langle \sigma_{22} \rangle_-^2}{E_{22}^0} + \frac{\sigma_{12}^2}{G_{12}^0(1-D_{12})} \right] \tag{9}$$

The energy expression (9) can be extended to a three-dimensional environment, by means of the assumption of a transverse isotropic behavior. It then regards that the internal variables affect the out-of-plane modules in the same way that the plane modules. The strain energy in the case of a ply in three-dimensional can then be written:

$$\begin{aligned} e_D = \frac{1}{2}\Bigg(& \frac{1}{(1-d_f)}\left[\frac{(\sigma_{11})^2}{E_{11}^0} - \left(\frac{\nu_{12}^0}{E_{11}^0} + \frac{\nu_{21}^0}{E_{11}^0} \right)\sigma_{11}\sigma_{22} - \left(\frac{\nu_{13}^0}{E_{11}^0} + \frac{\nu_{31}^0}{E_{33}^0} \right)\sigma_{11}\sigma_{33} - \left(\frac{\nu_{23}^0}{E_{22}^0} + \frac{\nu_{32}^0}{E_{33}^0} \right)\sigma_{22}\sigma_{33} \right] \\ & + \frac{\langle \sigma_{22} \rangle_-^2}{E_{22}^0} + \frac{\langle \sigma_{33} \rangle_-^2}{E_{33}^0} + \frac{1}{(1-d_{12})}\left[\frac{(\sigma_{12})^2}{G_{12}^0} + \frac{(\sigma_{23})^2}{G_{23}^0} + \frac{(\sigma_{13})^2}{G_{13}^0} \right] + \frac{1}{(1-d_{22})}\left[\frac{\langle \sigma_{22} \rangle_+^2}{E_{22}^0} + \frac{\langle \sigma_{33} \rangle_+^2}{E_{33}^0} \right] \Bigg) \end{aligned} \tag{10}$$

Where $E_{22}^0 = E_{33}^0, G_{12}^0 = G_{13}^0, \nu_{12}^0 = \nu_{13}^0, G_{23}^0 = E_{33}^0/(2(1+\nu_{23}))$. For a three-dimensional stress state

The formula shows on which terms of the stiffness are influenced by the damage. From this formula we derive the thermodynamic force vector $\boldsymbol{Y}$ conjugated to damage, in order to describe the initiation and progression of degradation mechanisms:

$$\mathbf{Y} = \frac{\partial \langle\langle \ e_D(\boldsymbol{\sigma}, \mathbf{D}) \ \rangle\rangle}{\partial \mathbf{D}} \tag{11}$$

Where the symbol $\langle\langle \bullet \rangle\rangle$ in equation (11) means the average value of the quantity $\bullet$ within the thickness. In the present study, the strain energy density is computed locally at each integration point across the ply thickness.

The activation of damage and its evolution is governed by the square root of a linear combination of the two thermodynamic forces Y_{22} and Y_{12}:

$$\overline{Y} = \sup_{\tau \le t}\left(\sqrt{Y_{12} + b_2 Y_{22}}\right) \tag{12}$$

Where b_2 is a coupling term between the transverse and shear damage. The variables Y_{22} and Y_{12} are defined according to relation (13):

$$\begin{aligned} Y_{22} &= \frac{\partial \langle\langle e_d \rangle\rangle}{\partial D_{22}} = \frac{\langle \sigma_{22} \rangle_+^2}{2(1-D_{22})^2 E_{22}^0}\left(\frac{\langle \sigma_{22} \rangle_+^2}{E_{22}^0} + \frac{\langle \sigma_{33} \rangle_+^2}{E_{33}^0}\right) \\ Y_{12} &= \frac{\partial \langle\langle e_d \rangle\rangle}{\partial D_{12}} = \frac{1}{2(1-D_{12})^2}\left(\frac{(\sigma_{12})^2}{G_{12}^0} + \frac{(\sigma_{23})^2}{G_{23}^0} + \frac{(\sigma_{13})^2}{G_{13}^0}\right) \end{aligned} \tag{13}$$

The transverse and shear damage variables D_{22} and D_{12} are defined as:

$$\Rightarrow D_{12} = \begin{cases} \dfrac{\left\langle \sqrt{\overline{Y}} - \sqrt{Y_{12}^0} \right\rangle_+}{\sqrt{Y_{12}^c} - \sqrt{Y_{12}^0}}, & \text{if } D_{12} < 1 \text{ and } Y_{12} < Y_{12}^c \\ 1 & \text{otherwise} \end{cases} \tag{14}$$

$$\Rightarrow D_{22} = \begin{cases} b_3 D_{12}, & \text{if } D_{22} < 1 \text{ and } Y_{22} < Y_{12}^c \\ 1 & \text{otherwise} \end{cases}$$

Where b_3 is a coupling term between the transverse and shear damages. Y_{12}^c and Y_{12}^0 are the limit strength for damage and the threshold strength for the initiation of damage, respectively. These material parameters are identified experimentally.

In addition to the above equations, the model is completed by a brittle failure criterion which takes into account failure of the fiber in tension and compression. This is governed by two critical damage thresholds Y_{11}^t and Y_{11}^c for the variable Y_{11}:

$$Y_{11} = \frac{\partial \langle\langle e_d \rangle\rangle}{\partial D_{11}} = \frac{1}{2(1-D_{11})^2}\left(\frac{(\sigma_{11})^2}{E_{11}^0} - \sum_{i=1}^{2}\sum_{j>i}^{3}\left(\frac{\nu_{ij}^0}{E_i^0} + \frac{\nu_{ji}^0}{E_j^0}\right)\sigma_{ii}\sigma_{jj}\right) \tag{15}$$

The damage fiber is introduced in the model, by considering the Young's modulus E_{11} as a nonlinear and it does depend on stresses σ_{11}:

$$\begin{cases} \text{if } \sigma_{11} > 0 \rightarrow \begin{cases} \text{if } Y_{11} > Y_{11}^t \ D_{11} = 1 \\ \text{otherwise } D_{11} = 0 \end{cases} \\ \text{if } \sigma_{11} < 0 \rightarrow \begin{cases} \text{if } Y_{11} > Y_{11}^c \ D_{11} = 1 \\ \text{otherwise } D_{11} = 0 \end{cases} \end{cases} \tag{16}$$

To limit the maximum damage rate and avoid numerical localization of damage, regularization parameters are introduced [13, 14], and the damage variables are corrected as below:

$$\dot{D}_{ij} = \frac{1}{\tau_c}\left(1 - e^{-a\left(D_{ij}^* - D_{ij}\right)}\right) \tag{17}$$

The same material constants, τ_c and a, are taken for the three damage evolution laws. For this model with delay effects, the variations of the forces Y_i do not lead to instantaneous variations of the damage variables D_i. There is a certain delay, defined by the characteristic

time τ_c.

3 ORTHOGONAL CUTTING MODELING APPROACHES

The simulation tests required by Taguchi method have been doing by using the finite elements software, Abaqus/Explicit [16]. The conception of the workpiece and, the information of the material mechanical properties have been informed in the Abaqus, while the damage behaviors have been implement by using a VUMAT subroutine [16]. Further information will be given in the following paragraphs.

3.1 Description of the model

Geometry and boundary conditions of the application are illustrated in Figure1. Nodes on the vertical lines, right and left, are constrained to move along the horizontal direction (X). Nodes on the horizontal bottom line are restrained to move along the horizontal and vertical directions, (X) and (Y) respectively. The values of cutting parameters and tool dimensions are chosen as those defined and used in [10] in order to validate predicted numerical results and experiments. The rake angle α is stated equal to 0°, the clearance angle γ is fixed at 11°, the tool edge radius r_ε is equal to15 µm, the depth of cut a_p = 0.2 mm. The cutting speed V_c is about 60 m/min.

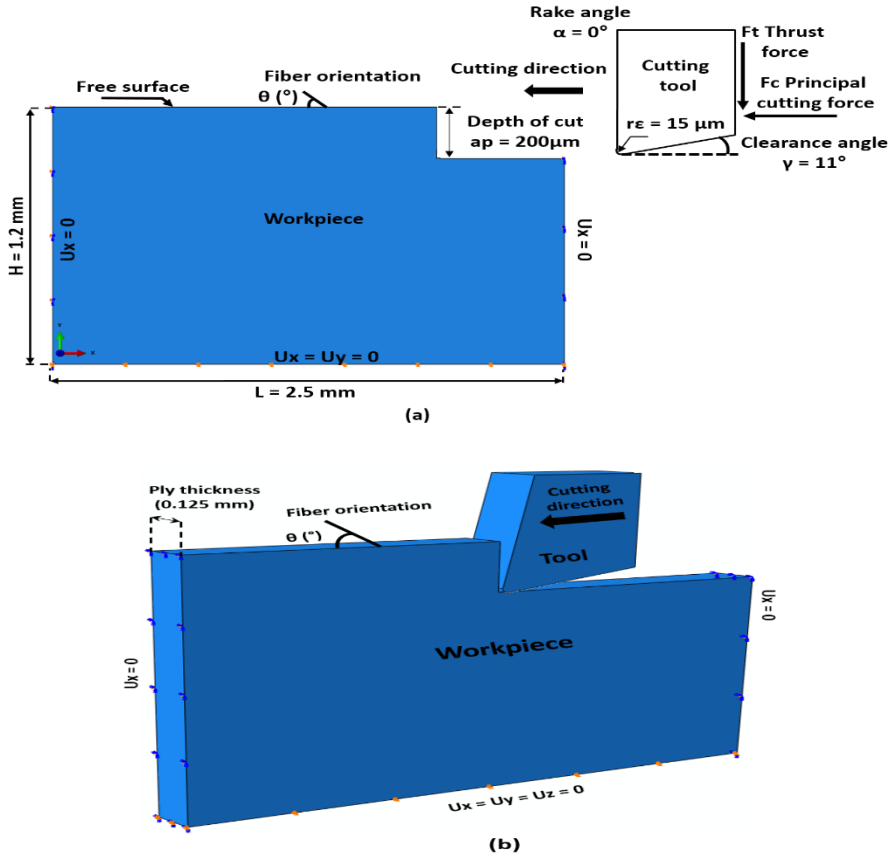

Figure 1: (a) Boundary condition and dimensions of the workpiece and the cutting tool for (a) 2D Model and (b) 3D Model

The tool is modelled as a rigid body and controlled by a reference point, where the cutting speed is applied and the machining forces are measured as reaction forces in output. The properties of a CFRP ply of T300/914 composites are taken from the work of Iliescu et al. [10] and remembered in Table 1. The workpiece is considered as a homogeneous equivalent material (HEM) with a longitudinal modulus in the fiber direction more than ten times higher than the transverse modulus.

The numerical simulation is done using Abaqus/Explicit code. A 2D model is conducted considering plane stress assumption and using continuum solid elements CPS4R available within Abaqus, with a linear (first-order) interpolation, and including automatic hourglass control, with reduced integration.

Table 1: Mechanical properties of the Aeronautical CFRP composite T300/914, [10]

$E_1^0\,(MPa)$	136600
$E_2^0\,(MPa)$	9600
$G_{12}^0\,(MPa)$	5200
ν_{12}^0	0.29
ν_{23}^0	0.4
ρ (Kg/m^3)	1578

The near zone of the tool where the chip will be formed was finely meshed. In a previous work, soldani et al.[9] proved that when the element size was less than or equal 7 µm, the differences in numerical results is negligible. Therefore, the size of the elements in this zone is of 5µm for 2D model and 8 µm for 3D model. While the remaining part is meshed coarsely with an element size in the range of 5 µm in the vicinity of the finely meshed area and 50 µm on the edges of the workpiece, see Figure 2.

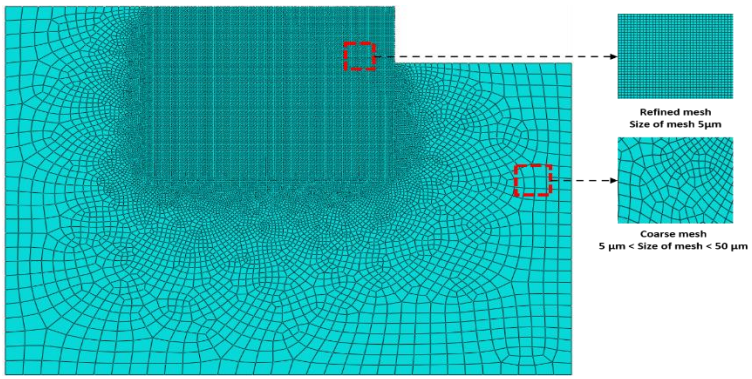

Figure 2: Used mesh for a fiber orientation of 45°

A VUMAT subroutine, providing a very general capability for implementing elastoplastic damage models, is used in Abaqus/Explicit. In addition, the element deletion approach is applied to represent the process of chip formation based on initiation and damage evolution in the workpiece. The set of the plastic-damage model parameters reported by Daghia et al.[15] have been adopted for the simulations in this work (Table 2).

The interaction between the node set of the workpiece surface and the tool surface is modeled

using surface-to-surface contact algorithm coupled to kinematic predictor/corrector contact algorithm with finite sliding formulation which are available in Abaqus/Explicit package. This approach allows to have a constant contact between the tool and the workpiece and this in spite the use of the "element deletion" option that eliminate the most damaged elements. The latter allows to have the chip formation.

Table 2: Plastic and damage parameters of UD-CFRP T300/914

Damage parameters [15]	
$Y_{12}^{C}\,(MPa)$	7
$Y_{12}^{0}\,(MPa)$	0
b	1
$Y_{11}^{t}\,(MPa)$	20
$Y_{11}^{c}\,(MPa)$	8
a	1
$\tau_c\,(\mu s)$	6
Plastic parameters	
α	0.42
$\beta\,(MPa)$	570
c	0.6164
$R_0\,(MPa)$	20

The contact between the tool and the workpiece is done at two contact zones. The first is located between the cutting face and the produced chip. The second is located between the flank face and the machined surface. The interaction between surfaces (tool/workpiece) is controlled by the Coulomb friction law and the friction coefficient, μ, is assumed to be constant during the cutting operation, as in various numerical studies, Nayak et al. [6], Gopala et al. [7] and Lasri et al. [8]. In the present study, a coefficient of friction equal to 0.4 was used.

3.2 Results and discussion

In the following subsections, the numerical results obtained of the orthogonal cutting operation, with 2D and 3D models for three CFRP plates orientations 45°, 90° and -45° will be presented and compared to experimental results obtained by Iliescu et al. [10]. The details of the chips formation and damage development are also discussed.

a. Chip formation process

The mechanical properties of the element will degrade when one of the three damage variables increases because the elastic modulus E_{ij} and shearing modulus G_{ij} are directly coupled to the damage variables, see equations (9 and 10). Consequently, the element finds itself into loss of rigidity and until one of three damage variable reaches the maximum value of 1 which causes loss total rigidity of the module to which it has been coupled. The element with no stiffness can then be removed. This procedure allowed us to follow the propagation of the primary and secondary cracks up to the chip formation.

Figure 3 shows the state of damage caused by the cutting tool edge in the workpiece oriented at 45°during the machining operation. The chip is produced by a succession of two failures.

The first failure is called "primary failure", see Figure 3(a), and is caused by compression

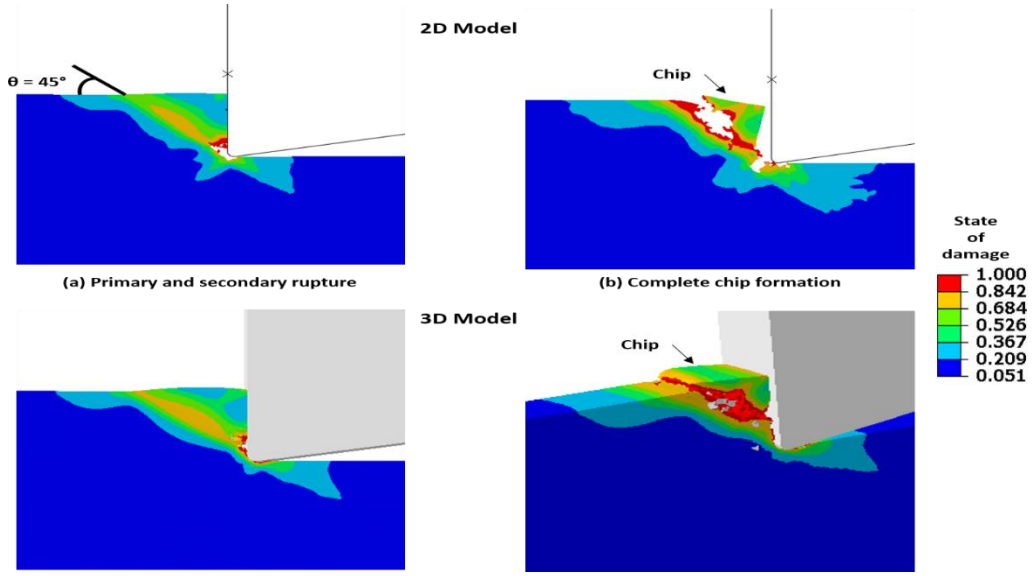

Figure 3: Progressive failure analysis of chip formation with 2D and 3D model for 45° fiber orientation (a) Primary rupture and Secondary rupture (b) Complete chip formation

induced shear perpendicular to the fiber axis, see Figure 3(a). The second failure is called secondary rupture. The latter is produced along the fiber/matrix interface, which is caused by the fiber-matrix debonding, see Figure 3(a), until it reaches the free surface of the workpiece forming then the complete chip, see Figure 3(b). These results are in good agreement with the experimental results of Iliescu [10], Wang et al [2] and Arola and Ramulu [3].

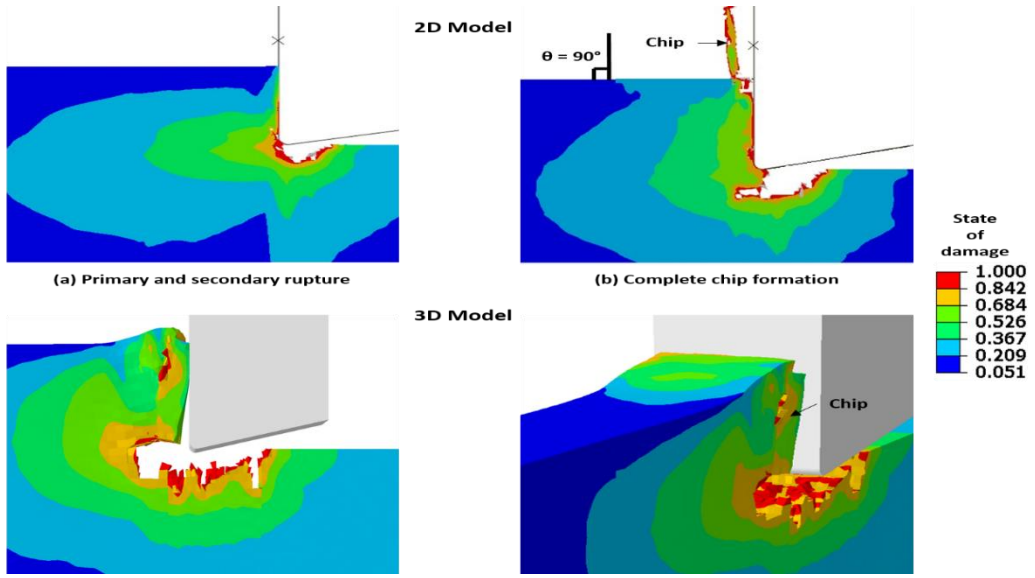

Figure 4: Progressive failure analysis of chip formation with 2D and 3D model for 90° fiber orientation (a) Primary rupture and Secondary rupture (b) Complete chip formation

For the 90° fiber orientation in Figure 4, the chip formation is also produced by a succession of two failures Figure 4(a). Primary failure is produced by tearing of fibers under the tool advancement. While the secondary rupture that propagates perpendicularly to the cutting direction is caused by the fiber-matrix debonding under the effect of shear stress. The latter propagates toward the free surface of the workpiece giving rise to the total chip formation Figure 4(b).

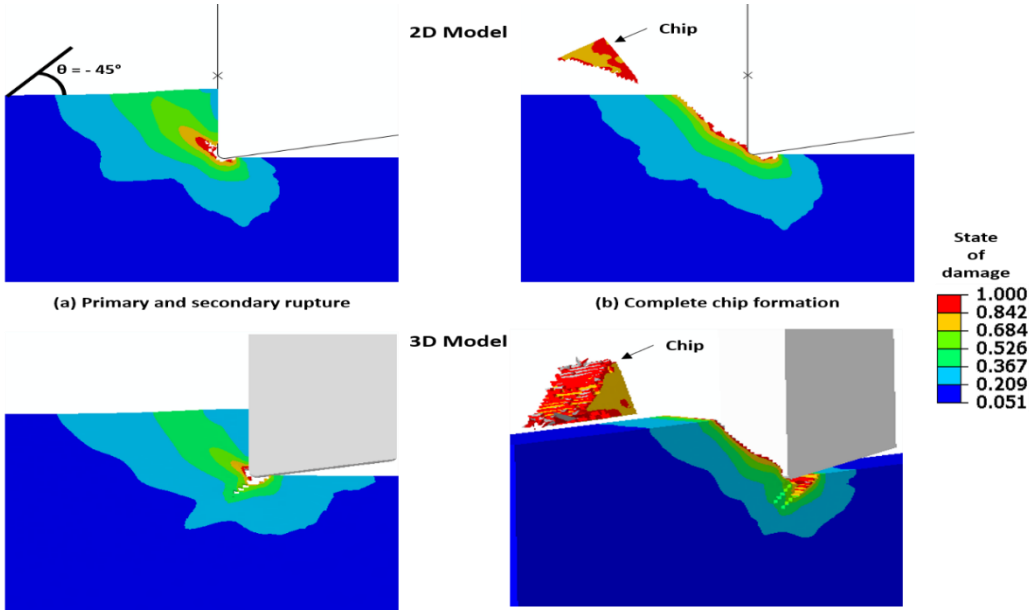

Figure 5: Progressive failure analysis of chip formation with 2D and 3D model for -45° fiber orientation (a) Primary rupture and Secondary rupture (b) Complete chip formation

For a fiber orientation at -45°, the chip formation is produced by a primary rupture along the fiber-matrix interface toward the interior of the workpiece. The fibers being negatively oriented, bend under the effect of the advancement of the cutting tool. Therefore a secondary rupture appears and takes the direction of the free surface, Figure 5(a). The total chip formation occurs when the secondary rupture reaches the free surface of the part as shown in Figure 5(b).

b. Prediction of cutting forces

Cutting forces are calculated at each increment of time during the displacement of the cutting tool following the cutting direction. The cutting force that is measured in the cutting direction, see Figure 1(a). The effect of the fiber orientation on cutting forces is carried forward on Figure 6. The conclusion that can be drawn from this graph is that the fiber orientation affects very significantly the cutting forces. The evolution of the cutting forces according the fiber orientation found in this study correlates with the findings made in different studies like Koplev et al. [1], Wang et al. [2], Arola et al. [3], and Iliescu et al. [10].

The values of the cutting force Fc obtained by simulations using the 2D model and 3D model for different orientations of fibers have the same values as those obtained experimentally by Iliescu [10], see Figure 6.

We note that the cutting forces Fc are important for orientation at 90° and -45°. This is explained by the fact that the fibers tend to bend before they are cut by the tool, therefore it requires cutting forces greater than for the orientation 45° where the chip formation is mainly due to the fiber-matrix debonding phenomenon.

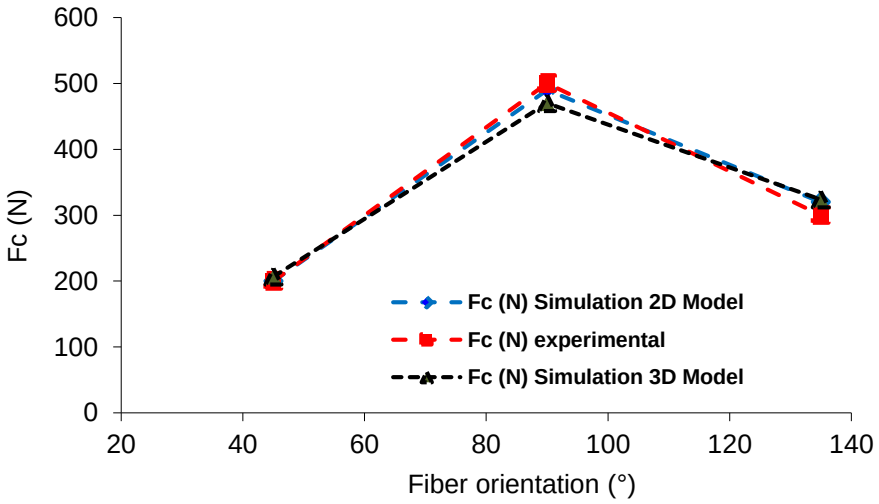

Figure 6: Cutting force Fc obtained during FE simulation for different fiber orientations with unidirectional composite compared with experimental results [10] (Vc = 60 m/min, ap = 0.2 mm, α=0°).

4 CONCLUSION

The main contribution of this paper is the development of a complete mechanical approach integrating coupling between damage and elastic-plastic behaviors to simulate the cutting process of FRP composites. The comparison of results obtained with this model and those obtained experimentally showed a realistic prediction of the proposed approach in terms of chip formation process, cutting forces and induced damage. The chip formation process can be clearly described and analyzed by the simulated physical mechanisms such as the primary and secondary ruptures.

The proposed model allows to predict accurate cutting forces as shown by the validation with experimental results taken from the literature.

From the results obtained in this work, the following conclusions can be drawn:

1. The complete mechanical approach integrating damaged elastic-plastic behaviour enables to offer another alternative to the traditional models used in the field of numerical simulation of machining composites, such as models including Hashin, Hoffman and Maximum stress criteria,
2. The current model can easily predict the induced subsurface damage and clearly show the influence of each cutting parameters and the fiber orientation on the machining process,
3. Finally, 90° fiber orientation was found by numerical simulation as the critical angle which generates severe subsurface damage. This fact was confirmed by all experimental studies reported by several authors in the literature.

REFERENCES

[1] Koplev, A. Lystrup, A. Vorm, T. The cutting process, chips and cutting forces in machining CFRP. Composites (1983) 14:371–376.

[2] Wang, D.H. Ramulu, M. Arola, D. *Orthogonal cutting mechanisms of graphite/epoxy composite. Part I: Unidirectional Laminate*. *Int J Mach Tool Manuf* (1995) 35:1623-1638

[3] Arola, D. Ramulu, M. Wang, D.H. *Chip formation in orthogonal trimming of graphite/epoxy*. *Compos: Part A* (1996) 27:121–133.

[4] Arola, D. and Ramulu, M. *Orthogonal cutting of fiber-reinforced composites: a finite element analysis. Int. J. Mech. Sci*.(1997) 39:597-613

[5] Zitoune, R. Collombet, F. Lachaud, F. Piquet, R. Pasquet, P. *Experimental calculation of the cutting conditions representative of the long fiber composite drilling Phase, Compos. Sci. Techno* (2005) 65:455-466.

[6] Nayak, D. Bhatnagar, N. Mahajan, P. *Machining studies of UD-FRP composites part 2: finite element analysis. Machining. Sci. Technol* (2005) 9:503-528

[7] Venu Gopala Rao, G. Mahajan, P. Bhatnagar, N. *Micro-mechanical modelling of machining of FRP composites-cutting force analysis. Compos. Sci. Techno* (2007) 67:579-593

[8] Lasri, L. Nouari, M. El-Mansori, M. *Modelling of chip separation in machining unidirectional FRP composites by stiffness degradation concept. Compos. Sci. Technol* (2009) 69:684-692.

[9] Santiuste, C. Soldani, X. Miguélez, H.M. *Machining FEM model of long fiber composites for aeronautical components, Compos Struct* (2010) 92:691-698.

[10] Iliescu, D. Gehin, D. Iordanoff, I. Girot, F. Gutiérrez, M.E. *A discrete element method for the simulation of CFRP cutting, Compos. Sci. Technol* (2010) 70:73-80.

[11] Ladeveze, P. and LeDantec, E. *Damage modelling of the elementary ply for laminated composites. Compos Sci Technol* (1992) 43:257-267.

[12] Lubineau, G. and Ladevèze, P. *Construction of a micromechanics-based intralaminar mesomodel, and illustrations in ABAQUS/Standard. Comput. Mater. Sci* (2008) 43:137-145.

[13] Ladevèze, P. Allix, O. Deü, J.F. Lévêque, D. *A mesomodel for localisation and damage computation in laminates. Comput Meth Appl Mech Engrg* (2000) 183:105–122.

[14] Allix, O. Feissel, P. Thévenet, P. *A delay damage mesomodel of laminates under dynamic loading basic aspects and identification issues. Comput Struct* (2003) 81:1177 –1191.

[15] Daghia, F. Ladevèze, P. Bordeu, F. Petiot, C. *On the validation of a micromechanics-based mesomodel for the simulation until failure of laminated composites. Comptes Rendus des JNC 16 Toulouse* 2009.

[16] Hibbitt, Karlsson. and Sorensen Inc. *ABAQUS version 6.11*; 2011.

[17] Lemaitre, J. and Chaboche, J.L. *Mechanics of Solid Materials, Cambridge University Press, Cambridge, UK* 1990

[18] Crisfield, M.A. *Non-Linear Finite Element Analysis of Solids and Structures. Vol 1: essentials* 1991